

Single-scattering characteristics of melting ice crystal particles in the millimeter-wave band

Xue-Hai Zhang(张学海), Wen-Bo Liu(刘文博), Xin-Hui Zhang(张欣慧), He-Li Wei(魏合理), Wei-Dong Li(李卫东), Jin-Long Duan(段金龙), Shu-Guang Zou(邹曙光), Jia Liu(刘佳), and Cong-Ming Dai(戴聪明)

Citation: Chin. Phys. B, 2025, 34 (**5**): 050307. DOI: 10.1088/1674-1056/adbd23
Journal homepage: http://cpb.iphy.ac.cn; http://iopscience.iop.org/cpb

What follows is a list of articles you may be interested in

Floquet scattering through a parity-time symmetric oscillating potential

Xuzhen Cao(曹序桢), Zhaoxin Liang(梁兆新), and Ying Hu(胡颖)
Chin. Phys. B, 2023, 32 (**3**): 030302. DOI: 10.1088/1674-1056/aca39a

Pseudospin symmetric solutions of the Dirac equation with the modified Rosen—Morse potential using Nikiforov—Uvarov method and supersymmetric quantum mechanics approach

Wen-Li Chen(陈文利) and I B Okon
Chin. Phys. B, 2022, 31 (**5**): 050302. DOI: 10.1088/1674-1056/ac2f33

Double differential cross sections for ionization of H by 75 keV proton impact: Assessing the role of correlated wave functions

Jungang Fan(范军刚), Xiangyang Miao(苗向阳), and Xiangfu Jia(贾祥福)
Chin. Phys. B, 2020, 29 (**12**): 120301. DOI: 10.1088/1674-1056/abb7f8

Exact scattering states in one-dimensional Hermitian and non-Hermitian potentials

Ruo-Lin Chai(柴若霖), Qiong-Tao Xie(谢琼涛), Xiao-Liang Liu(刘小良)
Chin. Phys. B, 2020, 29 (**9**): 090301. DOI: 10.1088/1674-1056/ab928f

Single-photon scattering controlled by an imperfect cavity

Liwei Duan(段立伟), Qing-Hu Chen(陈庆虎)
Chin. Phys. B, 2020, 29 (**7**): 070301. DOI: 10.1088/1674-1056/ab90ee

---

Single-scattering characteristics of melting ice crystal particles in the millimeter-wave band

Xue-Hai Zhang(张学海)[1], Wen-Bo Liu(刘文博)[1], Xin-Hui Zhang(张欣慧)[1], He-Li Wei(魏合理)[2], Wei-Dong Li(李卫东)[1], Jin-Long Duan(段金龙)[1], Shu-Guang Zou(邹曙光)[1], Jia Liu(刘佳)[3], and Cong-Ming Dai(戴聪明)[2,4,†]

[1] *School of Information Science and Engineering, Henan University of Technology, Zhengzhou* 450001, *China*
[2] *Key Laboratory of Atmospheric Optics, Anhui Institute of Optics and Fine Mechanics, Chinese Academy of Sciences, Hefei* 230031, *China*
[3] *College of Quality and Technical Supervision, Hebei University, Baoding* 071002, *China*
[4] *Advanced Laser Technology Laboratory of Anhui Province, Hefei* 230037, *China*

(Received 7 November 2024; revised manuscript received 20 January 2025; accepted manuscript online 6 March 2025)

The melting process of ice crystal particles has a significant effect on weather forecasting and global climate. Millimeter waveband is an excellent frequency range for exploring the optical characteristics of ice crystal particles. In this study, a new nonspherical and inhomogeneous ice crystal particle model is built based on the melting process of ice crystal particles. The single-scattering characteristics of ice crystal particles with different frequencies, sizes, shapes and ice crystal content (ICC) are investigated using the discrete dipole approximation (DDA) method. The results show that the single-scattering characteristics of ice crystal particles are closely related to the equivalent radius, frequency, morphology and mixing state. The single-scattering properties of the particles change regularly with the melting process of the ice crystal particles. Specifically, in the early stage of the ice crystal particle melting process, the single-scattering characteristics of ice crystal particles change significantly. With further melting, the change in the single-scattering characteristics of ice crystal particles gradually slows down when the ICC is less than 0.5. The results also show that in the early stage of the melting process, the shape of the ice crystal particles has a huge influence on the single-scattering characteristics of the particles, and in the late stage of the melting process, the single-scattering characteristics of the ice crystal particles are basically independent of the morphology of the ice crystal nuclei. This means that the influence of the morphology of the ice crystal nuclei needs to be considered in phases when simulating the scattering characteristics of the melting ice crystal particles. In summary, the results of this study should improve our understanding of the effect of size parameter, morphology and mixing state on the millimeter-wave scattering characteristics of ice clouds during the melting process and provide a reference for the remote sensing inversion of ice cloud microphysical characteristics.

Keywords: single-scattering characteristics, discrete dipole approximation, non-spherical ice crystal particles

PACS: 03.65.Nk, 07.57.Hm, 91.40.Dr, 95.30.Jx

DOI: 10.1088/1674-1056/adbd23 **CSTR:** 32038.14.CPB.adbd23

1. Introduction

Cirrus clouds cover approximately 20%–30% of the Earth's surface, with their coverage reaching 60%–70% in low tropical latitudes.[1] These clouds significantly influence the radiative balance of the Earth's atmospheric system by reflecting and absorbing both solar and terrestrial energy.[2–4] Composed primarily of non-spherical ice crystal particles that vary in size, morphology and mixing state, cirrus clouds exhibit complex physical processes. This complexity can elevate the uncertainty in assessing radiative forcing and climate change impacts.[5,6] Therefore, to mitigate this uncertainty, it is crucial to gain a deeper understanding of the cloud-physical processes and to precisely characterize the optical characteristics of cirrus clouds.[7–9]

The melting of ice crystal particles in cirrus clouds is a relatively common yet significant phenomenon.[10,11] It is necessary to study the effect of changes in the microphysical characteristics of ice crystal particles on their optical characteristics. However, most existing research on ice crystal melting has concentrated on ground-based precipitation, neglecting the unique behavior of ice crystal particles in high-altitude cirrus clouds. During the melting process of cirrus ice crystal particles, their microphysical characteristics, such as morphology and mixing state, experience intricate changes, which makes it very difficult to accurately simulate their single-scattering characteristics.[12,13] Therefore, it is essential to create an exact particle model and precisely characterize the single-scattering characteristics of ice crystal particles during the melting process.

Significant progress has been made in studies concerning the single-scattering characteristics of non-spherical ice crystal particles. Numerous ice crystal models have been developed and employed to examine the scattering characteristics of cirrus clouds. For example, Liu[14] investigated the single-scattering characteristics of ice crystal particles with

†Corresponding author. E-mail: cmdai@aiofm.ac.cn

© 2025 Chinese Physical Society and IOP Publishing Ltd. All rights, including for text and data mining, AI training, and similar technologies, are reserved.

11 different geometries in the microwave band. Kim[15] analyzed the single-scattering characteristics of ice crystals with five distinct shapes at frequencies of 94 GHz, 183 GHz and 340 GHz. Teschl *et al.*[16] extended this investigation to calculate the single-scattering parameters of frozen nonspherical water vapor condensates from 1 GHz to 300 GHz. However, ice crystal particle models are usually based on homogeneous equivalents. In reality, the mixing state of ice crystal particles during the melting process is typically inhomogeneous, potentially leading to substantial errors when utilizing homogeneous equivalent models. To address this issue, several studies have constructed models to investigate the changes in the scattering characteristics of ice crystal particles at different stages of melting. Sun *et al.*[17] proposed an external mixture model of spherical water and column particulate to simulate surface snowmelt particles. Leinonen and von Lerber[18] improved a three-dimensional model for melting single snowflakes. The change in the shape of the snowflake during the melting process is simulated, but this melting process cannot be parameterized. Johnson *et al.*[19] developed a single particle melting model (SPMM). Implementing and mapping into any existing thermodynamic/melting-layer model is easy. However, it only focuses on the initial range of melting (liquid volume fractions less than 0.15). Ori *et al.*[20] examined the applicability of the discrete dipole approximation (DDA) to partially melted snowflake scattering in the microwave band, utilizing a simple model of liquid water-coated ice spheres. Arreyndip and Joseph[21] compared the scattering abilities of different aerosol species. However, this simply divides the ice crystal melting process into droplets, ice water, melting ice (wet ice) and dry ice. However, it should also be recognized that most of the current ice crystal particle models have not fully considered the effect of the morphological and inhomogeneous characteristics of melting ice crystal particles, which may affect the accuracy and reliability of simulation results. Meanwhile, in satellite remote sensing research, a simple model is needed to meet the simulation needs of various situations while ensuring relatively low inaccuracy.

Many satellites carry satellite detectors in the frequency range of 85–190 GHz, which are sensitive to ice clouds.[22,23] At the same time, these frequencies, associated with higher frequencies (e.g., 220 GHz and 340 GHz), are used for the study of the optical and microphysical properties of ice clouds.[24–26] This paper aims to develop a new non-spherical and inhomogeneous model of ice crystal particles to examine the effect of morphology and inhomogeneous characteristics on the single-scattering characteristics during the melting process at three selected frequencies: 92 GHz, 220 GHz, 340 GHz. Section 2 outlines the methods and the models of melting ice crystals utilized in this research. The simulation and validation of the DDA are carried out in Section 3, and then the impact of particle morphology and mixing state parameters on the scattering characteristics of ice crystal particles throughout the melting process is investigated. Finally, Section 4 provides a comprehensive summary and discussion of the findings.

2. Methods

2.1. Discrete dipole approximation

The discrete dipole approximation (DDA), a flexible technique that accurately computes light scattering by arbitrarily shaped and inhomogeneous particles,[27] is used to calculate the single-scattering characteristics of the nonspherical ice crystals. In the DDA method, an array of polarizable point dipoles represents the continuum arbitrarily shaped target. The scattering characteristics of the specific target are calculated by the interaction between the array of dipoles and a monochromatic plane wave incident from infinity.[28] The main advantage of the DDA method is that it is completely flexible regarding the geometry of the target.[29]

To adequately satisfy the accuracy requirement of discrete dipole scattering (DDSCAT), it is necessary to meet the conservation criterion[30–33]

$$|m|kd < 1, \tag{1}$$

where m is the complex refractive index of ice/water particles, $k = 2\pi/\lambda$, λ is the wavelength and d is the dipole spacing. In this study, we require $|m|kd < 0.5$ to ensure the computational accuracy. For all particles, there are enough dipole numbers to describe the particle morphology. For the three space orientation angles, due to the spatial rotational symmetry of particles, we set β, Θ and Φ to run from $0 < (\beta, \Theta, \Phi) < 90^\circ$ with $N = 10$ intervals. We consider that these parameter settings are sufficient to ensure the accuracy of the calculation results.

In this study, we use the volume equivalent radius a_{eff} to describe the effective size of the particles, and the equivalent radius a_{eff} is defined as follows:

$$a_{\text{eff}} = (3V/4\pi)^{1/3}, \tag{2}$$

where V is the volume of non-spherical particles.

2.2. Microphysical and optical parameters

The extinction efficiency factor Q_{e}, absorption efficiency factor Q_{a}, scattering efficiency factor Q_{s}, single-scattering albedo ω and asymmetry factor g of the ice crystal particles are the most critical optical parameters that determine the radiative characteristics of cirrus. These parameters are dictated by the microphysical characteristics of the cirrus, such as the particle dimension D, cross-sectional projected area A and the complex refractive index of the particle. The integral optical characteristics of the cirrus can be obtained from the optical

characteristics of individual particles when the spectral distribution of the ice crystal particles is known. The particle size distribution of the ice crystal particles is given by[34]

$$n(D) = N_0 D^{\mu} \exp(-\kappa D), \tag{3}$$

where N_0 is the intercept, μ is the dispersion and κ is the slope. κ can be expressed as

$$\kappa = \frac{b+\mu+0.67}{D_{\mathrm{m}}}, \tag{4}$$

where D_{m} is the average maximum size of the particle and μ ranges from 0 to 2. Baum *et al.*[35] derived $b = 2.1$ for tropical ice clouds and $b = 2.3$ for mid-latitude ice clouds based on in situ data obtained from airborne sampling probes. In this study, the value of b is set at 2.2 and μ is set to 2 for the calculation.

Given the ice crystal particle size distribution, $n(D)$, the average scattering parameters can be calculated using the following equation:

Mean extinction efficiency:

$$\langle Q_{\mathrm{e}} \rangle = \frac{\int_{D_{\min}}^{D_{\max}} Q_{\mathrm{e}}(D) A(D) n(D)\,\mathrm{d}D}{\int_{D_{\min}}^{D_{\max}} A(D) n(D)\,\mathrm{d}D}; \tag{5}$$

Mean absorption efficiency:

$$\langle Q_{\mathrm{a}} \rangle = \frac{\int_{D_{\min}}^{D_{\max}} Q_{\mathrm{a}}(D) A(D) n(D)\,\mathrm{d}D}{\int_{D_{\min}}^{D_{\max}} A(D) n(D)\,\mathrm{d}D}; \tag{6}$$

Mean scattering efficiency:

$$\langle Q_{\mathrm{s}} \rangle = \frac{\int_{D_{\min}}^{D_{\max}} Q_{\mathrm{s}}(D) A(D) n(D)\,\mathrm{d}D}{\int_{D_{\min}}^{D_{\max}} A(D) n(D)\,\mathrm{d}D}; \tag{7}$$

Mean single scattering albedo:

$$\langle \omega \rangle = \frac{\int_{D_{\min}}^{D_{\max}} Q_{\mathrm{s}}(D) A(D) n(D)\,\mathrm{d}D}{\int_{D_{\min}}^{D_{\max}} Q_{\mathrm{e}}(D) A(D) n(D)\,\mathrm{d}D}; \tag{8}$$

Mean asymmetry factor:

$$\langle g \rangle = \frac{\int_{D_{\min}}^{D_{\max}} g(D) Q_{\mathrm{s}}(D) A(D) n(D)\,\mathrm{d}D}{\int_{D_{\min}}^{D_{\max}} Q_{\mathrm{s}}(D) A(D) n(D)\,\mathrm{d}D}. \tag{9}$$

2.3. Model for melting ice crystal particles

This study modeled pure ice crystal particles as hexagonal prisms, a common assumption in the ice cloud scattering characteristics simulation. In their study, Pan *et al.* found that hexagonal icicles have liquid surfaces during the melting process.[11] Jia *et al.*[36] and Shen *et al.*[37] showed that ice crystals begin to melt when the temperature reaches freezing point, generating a film of water that uniformly covers the surface of the ice crystals. Chen *et al.*[38] classified the melting of spherical ice crystal particles into three consecutive phases of ice crystals, ice-water mixing and water. Rodolfo and Marcelo[39] found that melting hexagonal ice columns have a thin liquid layer while the hexagonal cross-section of the columns is maintained during the melting process. Since a spherical shape has the most uniform heat-absorbing area, the melting of the icicle will eventually converge to a spherical shape and eventually melt into droplet particles. The melting process of these ice crystal particles can be systematically divided into five distinct stages, as shown in Fig. 1. At first, the particles are entirely ice crystals (Fig. 1(a)). When melting first begins, a thin hexagonal prismatic water film covers the surface of hexagonal ice crystal particles (Fig. 1(b)). With further melting, the shape of the water film changes from hexagonal prismatic to spherical (Fig. 1(c)). The shape of the ice crystals subsequently changes from hexagonal to spherical (Fig. 1(d)). Finally, the ice crystal particles completely melt into spherical water droplets (Fig. 1(e)).

The aspect ratio of ice crystal particles is given by $L/(2a)$, where L is the height of the hexagonal ice crystal particle and the length of the bottom edge of the hexagonal ice crystal particle model is a.

In this study, the ice crystal content (ICC) parameter is used to characterize the melting process of ice crystal particles during the melting process, which is defined as follows:

$$\mathrm{ICC} = \frac{V_{\mathrm{ice}}}{V_{\mathrm{ice}} + V_{\mathrm{water}}}, \tag{10}$$

where V_{ice} denotes the volume of ice crystal nuclei and V_{water} indicates the volume of water during the melting process. In reality, the melting process of ice crystal particles is a continuous process, and the morphology and mixing ratio of particle cores and shells are constantly changing. Therefore, the model constructed in this study can only roughly divide the melting of ice crystal particles into several stages with some errors, and then go on to study the stage-by-stage changes in the optical properties of the melted ice crystal particles. On this basis, this paper divides the ice crystal particle melting process into several stages.

When the ICC is 1, the particles are pure ice crystal particles (Fig. 1(a)); when the ICC is between 1 and 0.7, model 2 is used (Fig. 1(b)). In this range, the shape of the particle model does not change with the ICC. As the ICC changes, the size of the ice crystal nuclei changes, which reflects the result of the ICC change. When the ICC reaches a critical value, the model

shape changes to the shape of the next stage. After that, the model changes similarly; when the ICC is between 0.7 and 0.3, model 3 is used (Fig. 1(c)); when the ICC is between 0.3 and 0, model 4 is used (Fig. 1(d)); when the ICC = 0, the particles are completely melted into water droplet particles (Fig. 1(e)).

Oriented to the practical needs of remote sensing and detection, we need to construct an ice crystal model with simple parameterization and capable of describing the characteristics of a wide range of morphology and mixing state variations, which can simply and effectively characterize the optical properties of the melting ice crystal particles. From this aspect, the melting ice crystal particles constructed in the present study have a certain research value. The schematic table of model variation with ICC is as follows.

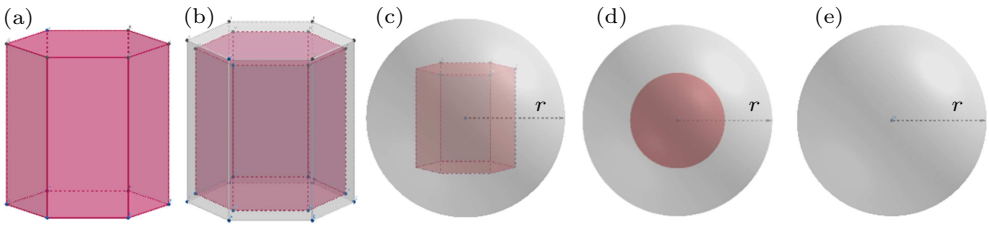
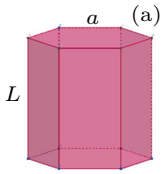
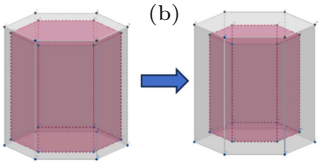
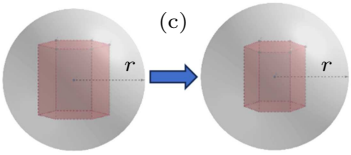
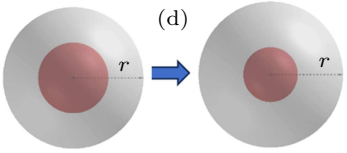
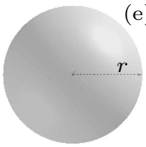


Fig. 1. Three-dimensional schematic diagram of the ice crystal particle model change process, (a)–(e) for the different stages of particle melting.

Table 1. Model variation with ICC.

ICC	Model schematic
1	
$0.7 < \text{ICC} < 1$	
$0.3 \leq \text{ICC} \leq 0.7$	
$0 < \text{ICC} < 0.3$	
0	

The refractive indices of the ice and water at frequencies of 92 GHz, 220 GHz and 340 GHz are shown in Table 2.[40,41]

Table 2. Complex refractive indices of ice and water at selected frequencies.[40,41]

Frequency (GHz)	Ice		Water	
	Real	Imaginary	Real	Imaginary
92	1.7864	0.0031410	3.4975	2.1615
220	1.7868	0.0051108	2.5575	1.3025
340	1.7889	0.0098112	2.3546	0.97192

3. Results

3.1. DDA simulation and validation of single-scattering characteristics of melting ice crystal particles

In this study, a model of melting ice crystal particles with model parameters of ICC = 0.1 and ICC = 0.5 is simulated using Mie scattering and DDA methods. The single-scattering characteristics (extinction efficiency, absorption efficiency, single-scattering albedo, asymmetry factor) of the melting ice crystal particles at 220 GHz are calculated using these two methods. The equivalent radius a_{eff} of the particles is 50–1000 μm. The results are shown in Fig. 2.

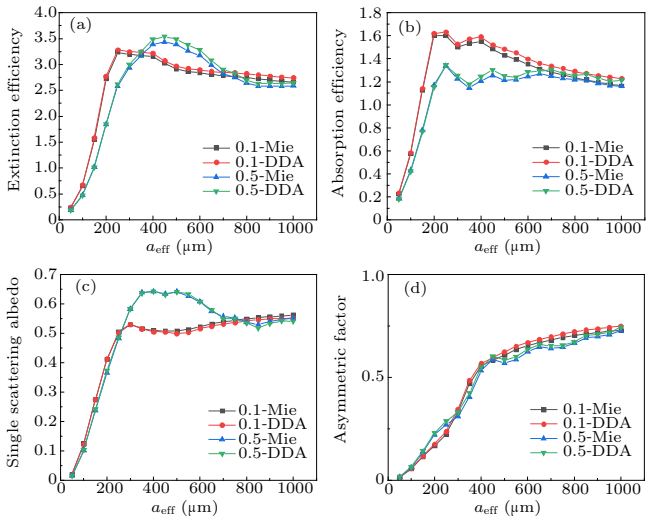


Fig. 2. Single-scattering characteristics of ice particles calculated by the DDA and Mie scattering methods.

As can be seen in Fig. 2, there are some differences in the results between the Mie scattering and DDA simulations, which is because the extinction and absorption efficiencies obtained by the DDA simulation of the melting of ice crystals at microwave frequencies are mainly dependent on the size of the dipole.[42]

Therefore, in this study, different numbers of dipoles are used to simulate the same shape of the model, and its single-scattering characteristics are calculated using the DDA method. As shown in Fig. 3, the simulation results are closer to the results of Mie scattering by increasing the number of dipoles to reduce the spacing between dipoles. It can also be seen that the accuracy of the dipole number 65117 used in this study can model the overall trend or difference between the two curves at ICC = 0.1 and ICC = 0.5. Therefore, the accuracy of the simulated data in this study can be guaranteed.

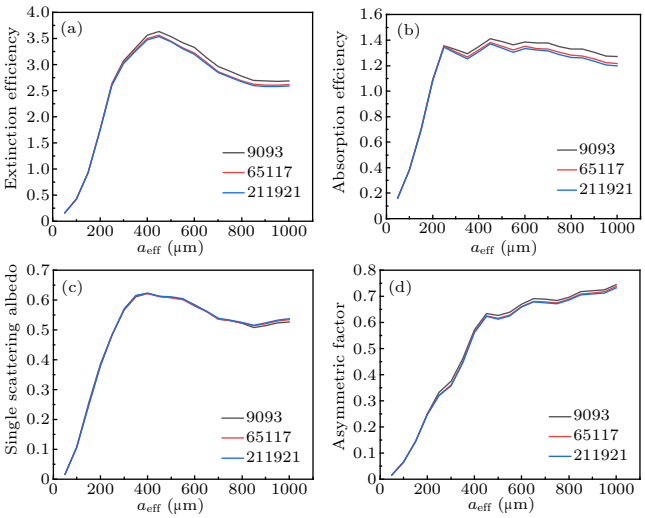


Fig. 3. Modelling melting ice crystal particles with different levels of discretization using DDA.

3.2. Effect of frequencies on the single-scattering characteristics of ice crystal particles and water droplet particles

In this subsection, the effect of frequencies on the single-scattering characteristics of ice crystal particles and water droplet particles are analyzed at three frequency bands, 92 GHz, 220 GHz and 340 GHz, as shown in Fig. 4.

Figure 4(a) shows that the extinction efficiency of the ice crystal particles displays a fluctuating variation with the particle equivalent radius, and the extinction efficiency of the water droplet particles shows a tendency to rapidly increase followed by stabilization with the increase in the particle equivalent radius.

Figure 4(b) shows that the absorption efficiency of ice crystal particles increases with increasing particle equivalent radius. Similarly, the absorption efficiency of water droplet particles shows a rapid increase with increasing particle equivalent radius, followed by a slow decrease. Furthermore, there is a correlation between frequency and the variation in absorption efficiency of ice crystal particles with particle equivalent radius, indicating that higher frequencies result in greater changes.

Figure 4(c) shows that the single-scattering albedos of ice crystal particles and water droplet particles at different frequencies rapidly increase with the equivalent radius of the particles before leveling off. Overall, the single-scattering albedo of ice crystal particles is approximately twice that of water droplet particles.

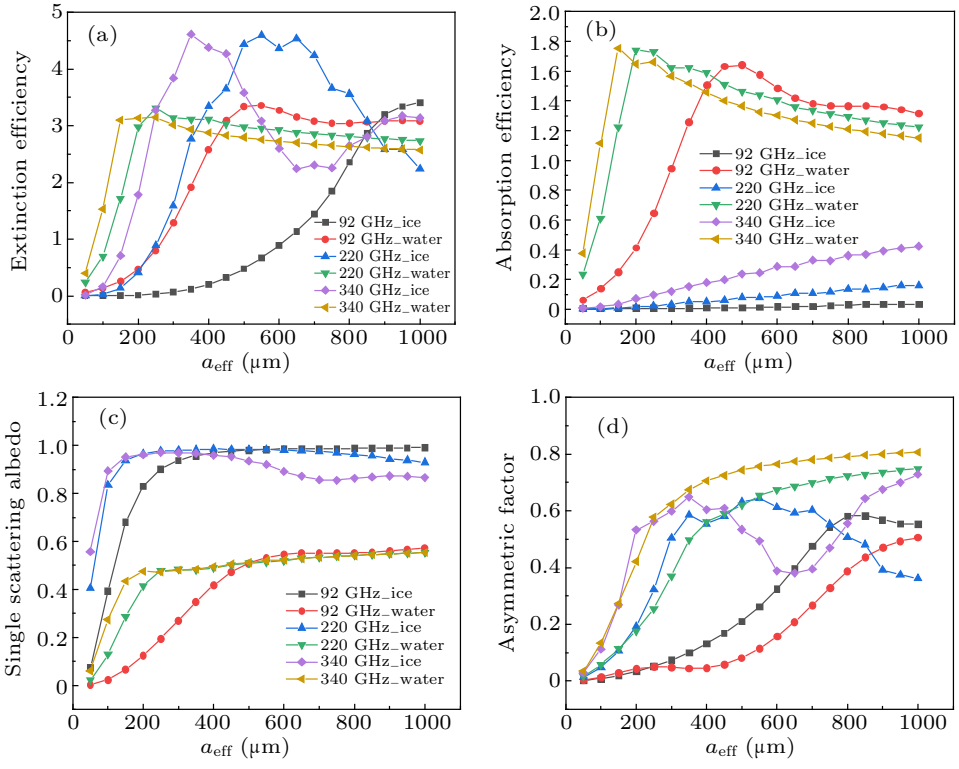


Fig. 4. Single-scattering parameters of water and ice crystal particles at the three selected frequencies.

Figure 4(d) shows that the asymmetry factor of the ice crystal particles displays a fluctuating variation with the particle equivalent radius. In contrast, the asymmetry factor of the water droplet particles increases with the increase in the particle equivalent radius.

In summary, analyzing single-scattering characteristics of water droplets and ice crystal particles in the 92 GHz, 220 GHz and 340 GHz bands provides valuable insight into quantitative remote sensing of ice crystal particles.

The average single-scattering parameters of water and ice crystal particles at the three selected frequencies are shown in Fig. 5. The difference between the average extinction efficiencies of water and ice crystal particles at 92 GHz is large, as depicted in Fig. 5(a). On the other hand, Fig. 5(b) illustrates significant differences in the average absorption efficiencies between ice crystal and water droplet particles. Specifically, the mean absorption efficiency of ice crystal particles increases with frequency, while water droplets reach their maximum mean absorption efficiency at 220 GHz. Figure 5(c) reveals that the average single-scattering albedo values of ice crystal particles at different frequencies are close to 1, slightly decreasing as the frequency rises. Conversely, water droplet particles have an average single-scattering albedo of approximately 0.5, which remains relatively stable with changing frequencies. Figure 5(d) shows that the average asymmetry factor of the water droplet particles increases with frequency, and the average asymmetry factor of the water droplet particles and ice crystal particles is the same at 220 GHz. These results indicate that the single-scattering properties of ice crystal particles are relatively sensitive to the 220 GHz frequency. Consequently, this frequency is selected for further investigation into the variations in the single-scattering characteristics of ice crystal particles during the melting process. The impact of ice crystal nuclei with different aspect ratios on the single-scattering characteristics of ice crystal particles during the melting process is also explored using 220 GHz.

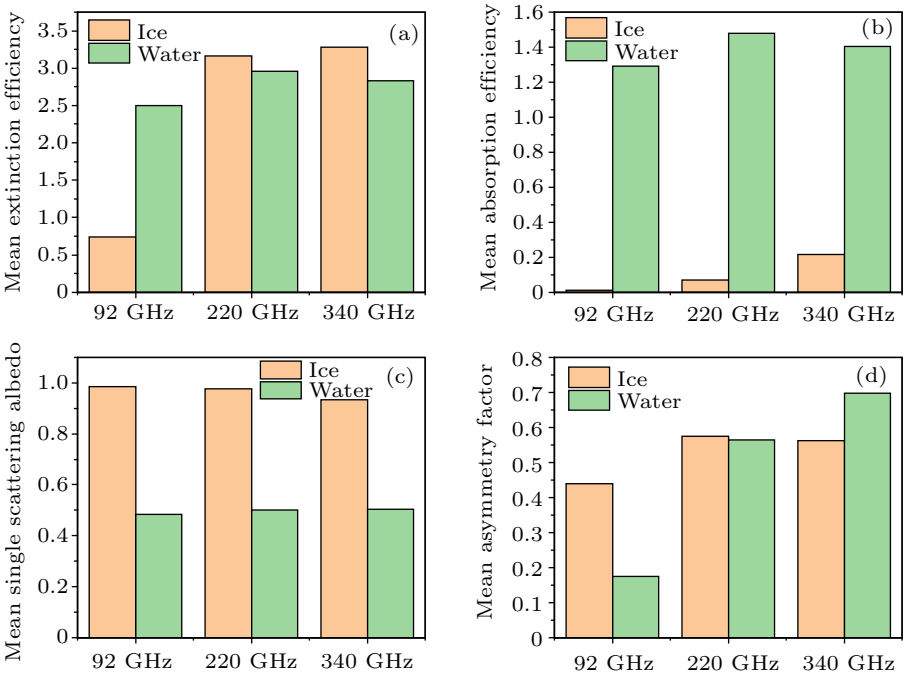


Fig. 5. Average optical property parameters of ice crystal particles and water droplet particles at different frequencies.

3.3. Influence of the melting process on the single-scattering characteristics

In this study, the changes in the scattering characteristics of ice crystal particles at different stages of melting are investigated based on the changes in ice crystal content during the melting process, and the results are shown in Fig. 6.

Figure 6(a) shows the variation in extinction efficiency with particle equivalent radius for ice crystal particles at different melting stages. In the early stage of melting, when the ICC is large, the extinction efficiency of the particles increases and then decreases with the increase in the particle equivalent radius. The magnitude of the change is large. In the late stage of melting, when the ICC is small, the extinction efficiency of particles increases rapidly. Then, it decreases slowly with the increase in the equivalent radius of particles, and the magnitude of the change is small.

Figure 6(b) shows the trend of particle absorption efficiency with equivalent radius at different melting stages. When the ICC is large, the particle absorption efficiency increases with the increase in the equivalent radius. However, when the ICC is small, the particle absorption efficiency increases rapidly with the increase in the equivalent radius, reaches a peak at the equivalent radius of 200 μm, and then decreases slowly. This indicates that the trend of particle ab-

sorption efficiency changes at different melting stages.

Figure 6(c) shows that, in the early stage of melting, the single-scattering albedo of ice crystal particles increases rapidly and then decreases slowly with an increase in the particle equivalent radius and reaches a peak value at the particle equivalent radius of 450 μm. In the late stage of melting, the single-scattering albedo of the ice crystal particles increases with an increase in the particle equivalent radius.

Figure 6(d) shows distinct variations in the asymmetry factor of ice crystal particles during the melting process. Initially, the asymmetry factor rises and falls as the particle equivalent radius increases, with the maximum value observed at a radius of 500 μm. Subsequently, as the melting progresses, the asymmetry factor exhibits a continuous increase correlated with the growth of the particles' effective radius. This dynamic behavior underscores the complexity of the melting process and its impact on the optical characteristics of ice crystals.

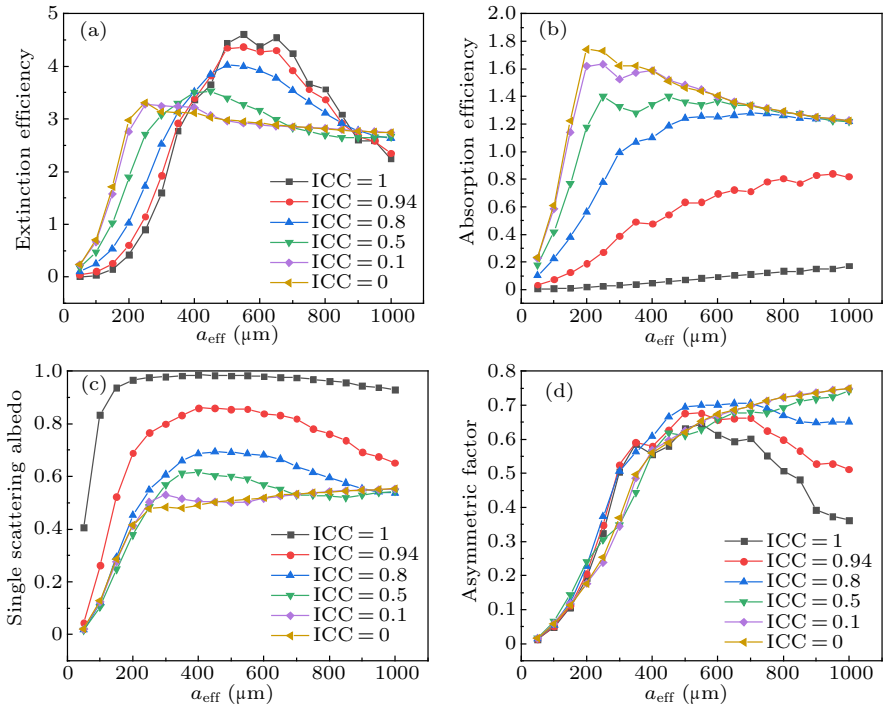


Fig. 6. Single-scattering parameters of melting ice crystal particles at different ICC.

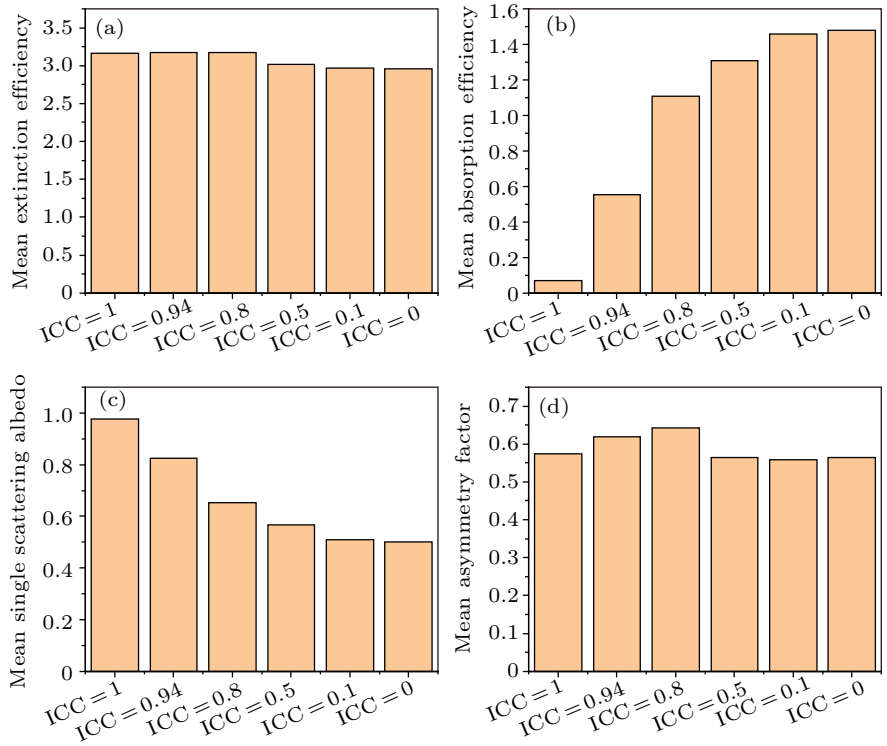


Fig. 7. Average optical property parameters of ice crystal particles during different melting processes.

During the melting process depicted in Fig. 7, the average optical property parameters of cirrus ice crystal particles exhibit distinct variations. As the melting process proceeds, the average extinction efficiency of the particle changes little, while the average absorption efficiency gradually increases. Simultaneously, the average single-scattering albedo shows a gradual decline from 1 to 0.5, indicative of alterations in the scattering and absorption characteristics. The average asymmetry factor reaches a maximum at ICC = 0.8, but the overall range in variation is limited. These observations suggest that variations in ICC have different effects on the single-scattering properties of particles. Specifically, the average absorption efficiency and single-scattering albedo are more influenced by ICC changes, whereas the average extinction efficiency and asymmetry factor demonstrate lower sensitivity to these variations. Consequently, monitoring changes in absorption efficiency and single-scattering albedo can aid in identifying the stage of the melting process in ice crystal particles, facilitating the assessment and inversion of microphysical characteristics in cirrus clouds.

3.4. Influence of ice crystal morphologies on the single-scattering characteristics

In this subsection, three aspect ratios, $L/(2a) = 0.33$, $L/(2a) = 1$ and $L/(2a) = 1.7$, are selected at an ICC of 0.4 to study the effect of the ice crystal nuclei's aspect ratio on the particles' single-scattering characteristics. At this point, the third stage of the model is used.

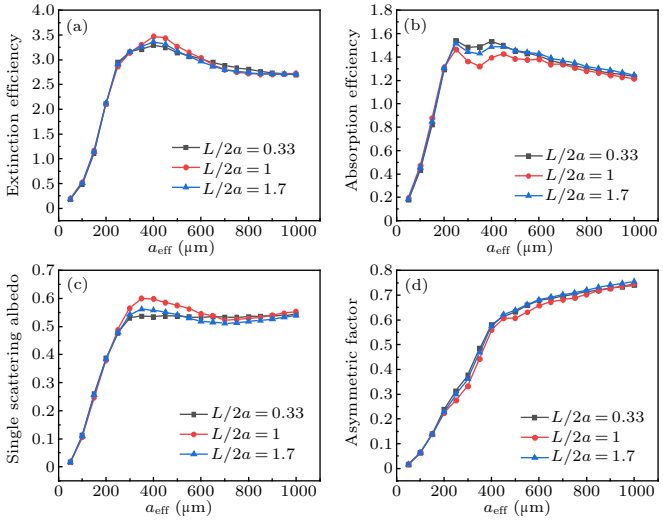


Fig. 8. Optical property parameters of ice crystal nuclei at different aspect ratios for an ICC of 0.4.

Figure 8 shows the effect of ice crystal nuclei with different aspect ratios on the single-scattering characteristics of the particles when the ICC is 0.4. This figure illustrates that the optical property parameters of the particles do not show significant changes collectively as the equivalent radius of the particles increases. This suggests that alterations in the aspect ratio of the ice crystal nuclei have minimal impact on the single-scattering characteristics of these particles.

The analysis presented in Fig. 9 indicates that variations in the aspect ratio of the ice crystal nuclei do not significantly impact the average optical property parameters of the cirrus ice crystal particles. From this, it can be inferred that alterations in the aspect ratio of the ice crystal particles do not substantially influence the overall average optical characteristics of the particles when the ICC is small.

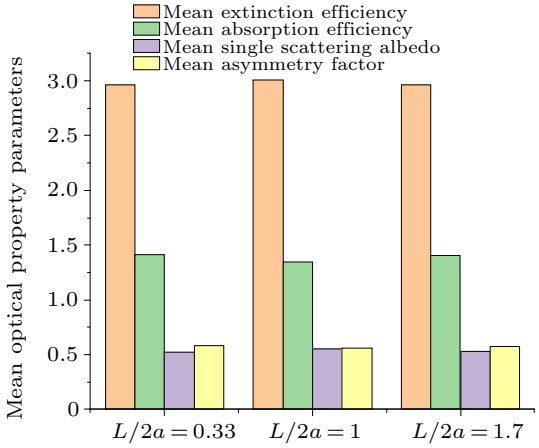


Fig. 9. Average optical property parameters of ice crystal particles at different aspect ratios for an ICC of 0.4.

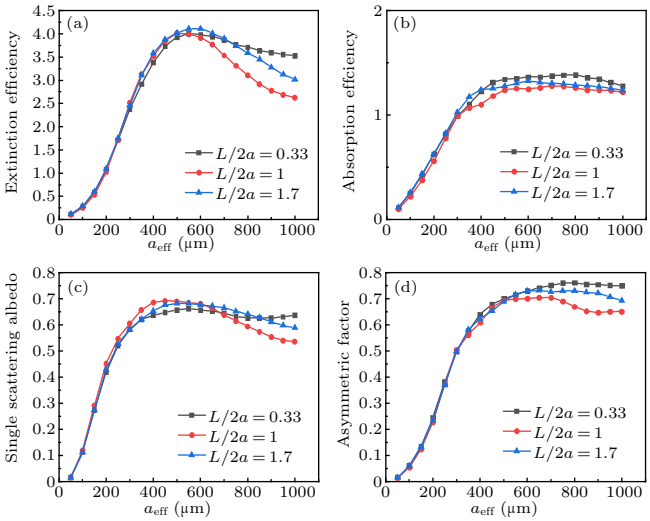


Fig. 10. Optical property parameters of ice crystal particles at different aspect ratios for an ICC of 0.8.

This study selects hexagonal prismatic ice crystal nuclei with aspect ratios of $L/(2a) = 0.33$, $L/(2a) = 1$ and $L/(2a) = 1.7$ when the ICC is 0.8 to explore whether different melting stages affect the conclusions drawn previously. It can be seen from Figs. 10 and 11 that there is a bright difference in the single-scattering characteristics of melted ice-crystal particles with different aspect ratios when the particle equivalent radius is larger than 500 μm, i.e., when the size parameter is larger than 2.5. Kim[15] examined the single-scattering characteristics of non-spherical ice-crystal particles at microwave frequencies ranging from 95–340 GHz. The results show that

the single-scattering characteristics of these particles are relatively unaffected by changes in the particle morphology parameter when the size parameter x ($x = 2\pi a_{\text{eff}}/\lambda$) is below 2.5. It is shown that this rule also applies to ice crystal particles in the pre-melting phase.

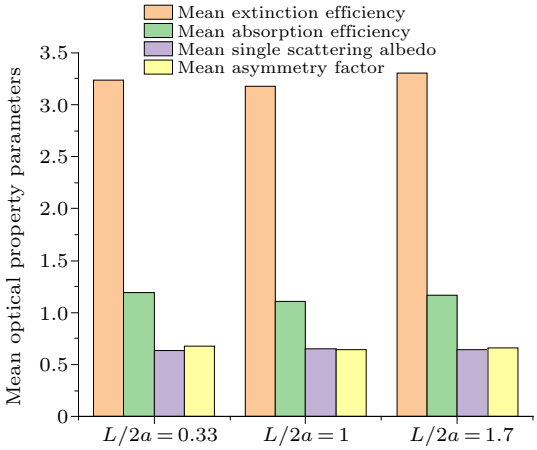


Fig. 11. Average optical property parameters of ice crystal particles at different aspect ratios for an ICC of 0.8.

4. Discussion

This study proposes a new inhomogeneous and nonspherical structure model for melting ice crystals into water droplet particles. The single-scattering characteristics of water and ice crystal particles at 92 GHz, 220 GHz and 340 GHz are investigated. The results indicate a significant influence of frequency and equivalent radius a_{eff} on the single-scattering characteristics of these particles. The melting ice particles' single-scattering characteristics strongly depend on the degree of melting during the melting process. The absorption efficiency and single-scattering albedo of the particles varied considerably at different levels of melting, and the variations were regular as the melting progressed. Meanwhile, the results show that the magnitude of the effect of particle morphology on the single-scattering characteristics of particles during the melting process of ice crystals depends on the particle scale parameter and the degree of melting. When the frequency is 220 GHz and the particle equivalent radius is less than 500 μm, the effect of particle morphology on the particle single-scattering characteristics is small at different stages of melting; when the particle equivalent radius is larger than 500 μm and ICC = 0.8, the effect of particle morphology on the particle single-scattering characteristics is significantly greater, and when ICC = 0.4, the effect of particle morphology on the particle single-scattering characteristics is relatively small. This finding helps model the melting process of ice crystal particles. Moreover, the investigation of the particles' optical and microphysical characteristics provides valuable insight into the significance of the results of our study.

It is essential to highlight that the ice crystal particle melting model developed in this study has limitations. Specifically, the model only accounts for the volume changes of ice crystals as they melt, and the morphology considerations are based solely on the impact of the aspect ratio variation of the ice crystal nucleus. This may result in significant deviations from the actual changes in the morphology of ice crystal nuclei during the melting process. It is crucial to address this limitation in future research by exploring the changes in ice crystal nucleus morphology to provide a more realistic explanation. Furthermore, it is essential to recognize that the ice crystal particle melting model presented in this study is an approximation aimed at illustrating the alterations in the single-scattering characteristics of ice crystal particles as they melt. The quantitative verifiability of the model is currently limited due to the lack of empirical results on melting ice crystals. Despite its limitations, the model holds promise for cirrus inversion and remote sensing applications. The results may be important for the detection of melting ice crystals and understanding the melting process of ice crystal particles. To enhance accuracy in describing particle size, morphology and mixing structure information, more precise ice crystal particle melting models must be developed. Looking ahead, our findings suggest the potential of the proposed model in guiding cirrus component retrieval and remote sensing studies using machine learning techniques. By leveraging these results, effective constraints can be established to improve the efficiency and accuracy of learning in these applications.

Acknowledgements

This study was supported by the National Key Research and Development Program of China (Grant No. 2019YFA0706004), the Key Projects of Science and Technology Research of Henan Province (Grant No. 222102320087), and the Key Scientific Research Project of Colleges and Universities in Henan Province (Grant No. 25B170004).

References

[1] Baran A J 2009 *Journal of Quantitative Spectroscopy and Radiative Transfer* **110** 1239
[2] Liu G 2004 *Journal of the Atmospheric Sciences* **61** 2441
[3] Um J, Jang S, Kim J, Park S, Jung H, Han S and Lee Y 2021 *Atmosphere* **31** 113
[4] Yang P, Liou K N, Bi L, Liu C, Yi B and Baum B A 2015 *Advances in Atmospheric Sciences* **32** 32
[5] Yang P, Liou K, Wyser K and Mitchell D 2000 *Journal of Geophysical Research: Atmospheres* **105** 4699
[6] Yang P, Wei H, Huang H L, Baum B A, Hu Y X, Kattawar G W, Mishchenko M I and Fu Q 2005 *Applied Optics* **44** 5512
[7] Krämer M, Rolf C, Spelten N, Afchine A, Fahey D, Jensen E, Khaykin S, Kuhn T, Lawson P and Lykov A 2020 *Atmospheric Chemistry and Physics* **20** 12569
[8] Magee N, Boaggio K, Staskiewicz S, Lynn A, Zhao X, Tusay N, Schuh T, Bandamede M, Bancroft L and Connelly D 2021 *Atmospheric Chemistry and Physics* **21** 7171
[9] Yang P, Bi L, Baum B A, Liou K N, Kattawar G W, Mishchenko M I and Cole B 2013 *Journal of the Atmospheric Sciences* **70** 330
[10] Maruyama M 2011 *Journal of Crystal Growth* **318** 36

[11] Pan D, Liu L M, Slater B, Michaelides A and Wang E 2011 *ACS Nano* **5** 4562

[12] Lu Y, Jiang Z, Aydin K, Verlinde J, Clothiaux E E and Botta G 2016 *Atmospheric Measurement Techniques* **9** 5119

[13] Szyrmer W, Tatarevic A and Kollias P 2012 *Journal of Geophysical Research: Atmospheres* **117** D14203

[14] Liu G 2008 *Bulletin of the American Meteorological Society* **89** 1563

[15] Kim M J 2006 *Journal of Geophysical Research: Atmospheres* **111** D14201

[16] Teschl F, Randeu W L and Teschl R 2009 *Atmospheric Research* **94** 564

[17] Sun W, Wielicki B A, Baize R R, Lukashin C, Hu Y, Zubko E, Videen G, Kim S S and Choi Y J 2019 *Journal of Quantitative Spectroscopy and Radiative Transfer* **222** 154

[18] Leinonen J and von Lerber A 2018 *Journal of Geophysical Research: Atmospheres* **123** 1811

[19] Johnson B, Olson W and Skofronick Jackson G 2016 *Atmospheric Measurement Techniques* **9** 9

[20] Ori D and Kneifel S 2018 *Journal of Quantitative Spectroscopy and Radiative Transfer* **217** 396

[21] Arreyndip N A and Joseph E 2024 *Opt. Express* **32** 4614

[22] Evans K F and Stephens G L 1995 *Journal of the Atmospheric Sciences* **52** 2041

[23] Wang J, Liu G, Spinhirne J, Racette P and Hart W 2001 *Journal of Geophysical Research: Atmospheres* **106** 15251

[24] Deeter M N and Evans K F 2000 *Journal of Applied Meteorology and Climatology* **39** 623

[25] Liu G and Curry J A 2000 *Journal of Applied Meteorology and Climatology* **39** 1318

[26] Miao J, Johnsen K P, Buehler S and Kokhanovsky A 2003 *Atmospheric Chemistry and Physics* **3** 39

[27] Draine B T and Flatau P J 1994 *J. Opt. Soc. Am. A* **11** 1491

[28] Draine B T and Flatau P J 2000 arXiv:astro-ph/0008151 [astro-ph]

[29] Hong G 2007 *Journal of Geophysical Research: Atmospheres* **112** D11208

[30] Draine B T and Flatau P J 2013 arXiv:1305.6497 [physics]

[31] Liu C, Bi L, Panetta R L, Yang P and Yurkin M A 2012 *Opt. Express* **20** 16763

[32] Podowitz D I, Liu C, Yang P and Yurkin M A 2014 *Journal of Quantitative Spectroscopy and Radiative Transfer* **146** 402

[33] Zhou C, Han X and Bi L 2023 *Opt. Express* **31** 24183

[34] Baum B A, Heymsfield A J, Yang P and Bedka S T 2005 *Journal of Applied Meteorology and Climatology* **44** 1885

[35] Baum B A, Yang P, Heymsfield A J, Platnick S, King M D, Hu Y and Bedka S T 2005 *Journal of Applied Meteorology* **44** 1896

[36] Jia W, Zhang F, Yang B W and Zheng M 2024 *Journal of Beijing University of Aeronautics and Astronautics* (in Chinese)

[37] Shen H, Han B B and Zhang L F 2020 *Journal of Experiments in Fluid Mechanics* **34** 1 (in Chinese)

[38] Chen J J, Liu X F, Zhong F H, Miao Q S, Zheng M, Wei Z and Hou Y 2023 *Transactions of Nanjing University of Aeronautics & Astronautics* **40** 653

[39] Pereyra R G and Carignano M A 2009 *The Journal of Physical Chemistry C* **113** 12699

[40] Segelstein D J 1981 *The complex refractive index of water* (Kansas: University of Missouri–Kansas City)

[41] Warren S G and Brandt R E 2008 *Journal of Geophysical Research: Atmospheres* **113** D14220

[42] Kanngießer F and Eriksson P 2022 *Opt. Lett.* **47** 4203